OClO slant column densities derived from GOMOS averaged transmittance measurements

C. Tétard, D. Fussen, F. Vanhellemont, C. Bingen, E. Dekemper, N. Mateshvili, D. Pieroux, Cédric Robert Robert, E. Kyrölä, J. Tamminen, et al.

Atmos. Meas. Tech., 6, 2953–2964, 2013
www.atmos-meas-tech.net/6/2953/2013/
doi:10.5194/amt-6-2953-2013

Atmospheric Measurement Techniques
Open Access

OClO slant column densities derived from GOMOS averaged transmittance measurements

C. Tétard[1], D. Fussen[1], F. Vanhellemont[1], C. Bingen[1], E. Dekemper[1], N. Mateshvili[1], D. Pieroux[1], C. Robert[1], E. Kyrölä[2], J. Tamminen[2], V. Sofieva[2], A. Hauchecorne[3], F. Dalaudier[3], J.-L. Bertaux[3], O. Fanton d'Andon[4], G. Barrot[4], L. Blanot[4], A. Dehn[5], and L. Saavedra de Miguel[6]

[1]Institut d'Aéronomie Spatiale de Belgique, Brussels, Belgium
[2]Finnish Meteorological Institute, Earth Observation, Helsinki, Finland
[3]Laboratoire Atmosphères, Milieux, Observations Spatiales, CNRS-INSU, Univ. Versailles St-Quentin, Guyancourt, France
[4]ACRI–ST, Sophia-Antipolis, France
[5]European Space Research Institute (ESRIN), European Space Agency, Frascati, Italy
[6]IDEAS, Serco, Frascati, Italy

Correspondence to: C. Tétard (cedric.tetard@aeronomie.be)

Received: 27 February 2013 – Published in Atmos. Meas. Tech. Discuss.: 11 April 2013
Revised: 20 September 2013 – Accepted: 30 September 2013 – Published: 4 November 2013

Abstract. The Global Ozone Monitoring by Occultation of Stars (GOMOS) instrument on board the European platform ENVISAT (ENVironment SATellite) was dedicated to the study of the of Earth's atmosphere using the stellar occultation technique. The spectral range of the GOMOS spectrometer extends from the UV (ultra violet) to the near infrared, allowing for the retrieval of species such as O_3, NO_2, NO_3, H_2O, O_2, air density, aerosol extinction and OClO. Nevertheless, OClO cannot be retrieved using a single GOMOS measurement because of the weak signal-to-noise ratio and the small optical thickness associated with this molecule. We present here the method used to detect this molecule by using several GOMOS measurements. It is based on a two-step approach. First, several co-located measurements are combined in a statistical way to build an averaged measurement with a higher signal-to-noise ratio; then, a differential optical absorption spectroscopy (DOAS) method is applied to retrieve OClO slant column densities (SCD). The statistics of the sets of GOMOS measurements used to build the averaged measurement and the spectral window selection are analyzed. The obtained retrievals are compared to results from two balloon-borne instruments. It appears that the inter-comparisons of OClO are generally satisfying (relative differences are about 15–60 %). Two nighttime climatologies of OClO based on GOMOS averaged measurements are presented. The first depicts annual global pictures of OClO from 2003 to 2011. From this climatology, the presence of an OClO SCD peak in the equatorial region at about 35 km is confirmed and strong OClO SCD in both polar regions are observed (more than 10^{16} cm^{-2} in the Antarctic region and slightly less in the Arctic region), a sign of chlorine activation. The second climatology is a monthly time series. It clearly shows the chlorine activation of the lower stratosphere during winter. Moreover the equatorial OClO SCD peak is observed during all years without any significant variations. This very promising method, applied on GOMOS measurements, allowed us to build the first nighttime climatology of OClO using limb-viewing instruments.

1 Introduction

The discovery of the stratospheric ozone depletion in Antarctica by Farman et al. (1985) has led to numerous studies to understand the physical and chemical mechanisms involved in this recurrent phenomenon. Halogen species play an important role in the chemical cycles that lead to polar ozone depletion (Solomon et al., 1986). Of these cycles, those involving active chlorine species (Cl, ClO, Cl_2O_2) are among the most efficient (Salawitch et al., 1993). The presence of chlorine species in the atmosphere is mainly due to the emission of chlorofluorocarbons (CFC) at the ground. CFCs are

chemically inert in the troposphere and are not soluble in water, which make them resistant to washout processes. Therefore, they are efficiently transported into the stratosphere where they are photolyzed by UV radiation or oxidized to produce atomic chlorine and chlorine monoxide (ClO). One consequence of the accumulation of ClO in the stratosphere is the formation of chlorine dioxide (OClO) via one of the possible reactions between ClO and bromine dioxide (BrO):

$$ClO + BrO \rightarrow OClO + Br, \quad (R1)$$

$$ClO + BrO \rightarrow BrCl + O_2, \quad (R2)$$

$$ClO + BrO \rightarrow Br + Cl + O_2. \quad (R3)$$

Thus, the detection of OClO in the stratosphere is a sign of chlorine activation. Also, nitrogen dioxide (NO_2) is of primary importance for polar ozone chemistry. Notably, in the presence of a third molecule (for example N_2 or O_2), NO_2 reduces the production of OClO by reacting with ClO or BrO to form inert chlorine and bromine reservoirs:

$$ClO + NO_2 + M \rightarrow ClONO_2 + M, \quad (R4)$$

$$BrO + NO_2 + M \rightarrow BrONO_2 + M. \quad (R5)$$

During the night, NO_2 reacts with nitrogen trioxide (NO_3) to form dinitrogen pentoxide (N_2O_5). The nighttime formation of N_2O_5 is responsible for the slow decrease of NO_2 and NO_3 during the night. Therefore in the wintertime's permanent night at high latitude regions, this reaction leads to the removal of almost all of NO_2 and NO_3: this is the well-known denoxification process. Subsequently, reactions (R4) and (R5) are very limited in the polar vortex (a large-scale region of air that is contained by a strong jet stream that circles the polar region) and OClO can then be formed via the reaction (R1). The concentration of OClO is determined by NO_2, ClO and BrO. Also, the process of denitrification (the permanent removal of reactive nitrogen from a certain altitude through sedimentation of HNO_3) must also be taken into account. Since HNO_3 is a reservoir species for NO_2, the denitrification leads to low NO_2 concentrations in the stratosphere and therefore reaction (R4) is also limited by this process. Consequently, OClO and NO_2 are expected to be anti-correlated in the polar regions. The OClO concentration is expected to remain constant during the night as the only sink of this species is the photolysis by solar radiation. The absorption cross section of OClO is characterized by strong differential structures in the near-UV range. This feature will also allow us to perform the retrieval of OClO. More details about stratospheric chemical processes involving chlorine and nitrogen species can be found in Solomon (1999).

Another important aspect of the OClO chemistry is its interactions with NO_2, which are not completely understood. A few studies have covered the subject (Riviere et al., 2003, Riviere et al., 2004, Berthet et al., 2007, Tetard et al., 2009) but all have concluded that uncertainties in the understanding of these interactions persist. It is therefore critical to monitor simultaneously OClO and NO_2. Previous OClO measurements have included the following:

- measurements using ground-based instruments or nadir-viewing satellite instruments allowing the retrieval of the vertical column of OClO (Solomon et al., 1987, Miller et al., 1999, Wagner et al., 2002 and Oetjen et al., 2011).

- measurements using balloon-borne instruments allowing the retrieval of the vertical profile of concentration of OClO: Absorption by the Minor components Ozone and NO_x (AMON, Renard et al., 1997), and Spectroscopie d'Absorption Lunaire pour l'Observation des Minoritaires Ozone et NO_x (SALOMON, Renard et al., 2000). In our study, flights of these two instruments have been used to compare the OClO concentration profiles retrieved from the Global Ozone Monitoring by Occultation of Stars (GOMOS) measurements (Bertaux et al., 2010).

- measurements using limb-scattered sunlight instruments allowing the retrieval of the OClO vertical distributions: Optical Spectrograph and InfraRed Imager System (OSIRIS; Krecl et al., 2006), and SCanning Imaging Absorption SpectroMeter for Atmospheric CHartographY (SCIAMACHY; Kühl et al., 2008). These measurements will not be used in our comparison study because GOMOS performs nighttime measurements. The comparison between these measurements performed under different illumination conditions requires the use of photochemical box model and will be done in an other study.

- measurements using lunar occultation instruments allowing the studies of the vertical profile of OClO concentrations: Stratospheric Aerosol and Gas Experiments III (SAGE III). However, no scientific studies about this have been published yet.

This represents a small and disjoint collection of observations compared to the large array of observations for species such as NO_2. GOMOS is the only satellite instrument able to perform nighttime measurements of the vertical distribution of OClO on a long term and on a global scale. Two previous studies about OClO retrieved using measurements from the GOMOS instrument have already been published: the first, by Fussen et al. (2006), has demonstrated the ability to retrieve OClO and has discovered the presence of an equatorial OClO SCD peak in the upper stratosphere; and the second, by Tetard et al. (2009), has illustrated the anti-correlation between OClO and NO_2 in the Arctic polar vortex only for

winters 2003–2008. Nevertheless, no extended climatology of stratospheric OClO from GOMOS has yet been published.

In this paper, we present the method used to retrieve OClO from GOMOS measurements. The method is an evolution of that described in Fussen et al. (2006). A more careful statistical processing has been applied and the spectral window has been optimized. Firstly, a statistical analysis is applied on several co-located GOMOS transmittance measurements to construct an averaged transmittance measurement; then, a DOAS (differential optical absorption spectroscopy) process based on these averaged measurements is applied to compute the slant column density (hereafter SCD) of OClO. Thereafter, the study focuses on the comparisons between the OClO GOMOS products and those retrieved using measurements from two different balloon-borne instruments. Finally, global annual and monthly climatologies of OClO are presented both in terms of SCDs and of concentrations.

This article focuses on the importance and the power of the use of averaged measurements to detect small absorbers.

2 The GOMOS instrument

The GOMOS instrument was onboard the European platform ENVISAT (ENVironment SATellite) in February 2002 on a heliosynchronous orbit at 800 km altitude and with an inclination of 98.55°. The GOMOS mission ended on April 2012 when contact with ENVISAT was lost. During its ten years of operation, GOMOS carried out about 860 000 occultations. The instrument operation is based on a grating spectrometer operating in stellar occultation mode: at each tangent altitude z and each wavelength λ, the transmittance $T(\lambda, z)$ is obtained by dividing the stellar radiance attenuated through the atmosphere $S(\lambda, z)$ by the reference star radiance $S_0(\lambda)$ measured outside the atmosphere. Thus, these measurements are self-calibrated and this is one of the main advantages of the method. Another advantage is related to the important number of light sources available (about 180 stars are used) that allows a global coverage in about three days (according to the mission baseline scenario). Nevertheless, some drawbacks of the stellar occultation method have to be mentioned. The selected stars have different magnitude, temperature and spectra with a clear impact on the signal-to-noise ratio of the measured spectra and therefore on the retrieval error budget. Moreover, the scintillation of stars has to be considered (Bertaux et al., 2010). It is due to small-scale vertical To overcome this problem, two fast photometers (with 1 kHz sampling rate) were installed in parallel to the spectrometers. However, it appears that the correction of the scintillation, while correct when the star setting is vertical (close to the orbital plane), is imperfect for oblique occultations (Sofieva et al., 2009). In this case, residual scintillation persists due to atmospheric inhomogeneous horizontal structures. Figure 1 shows an example of transmittance spectra obtained from oblique (top panel) and vertical (middle panel) occultations.

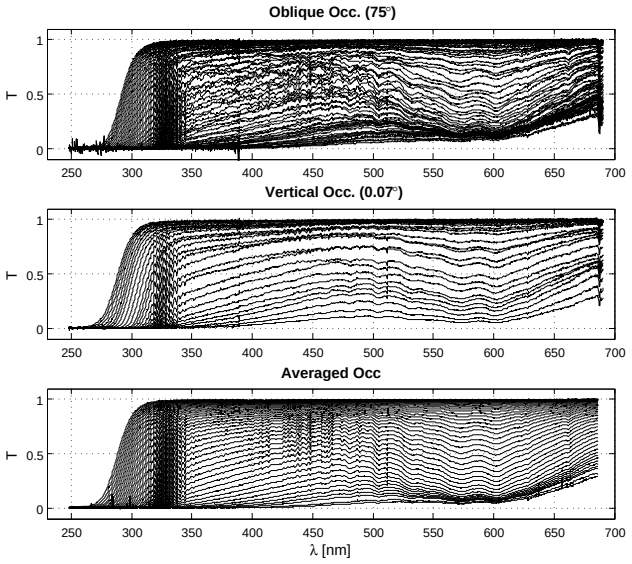

Fig. 1. Example of GOMOS transmittance spectra for an oblique occultation (top panel), a vertical occultation (middle panel) and an averaged occultation (bottom panel). The altitude range is 15–60 km.

The presence of residual scintillations is clearly visible in the spectra from oblique occultation whereas scintillation is almost perfectly removed in the spectra from vertical occultation. The vertical resolution is 1.7 km for vertical occultations and better for oblique ones.

GOMOS comprises four spectrometers: the two first in the UV–visible spectral range (from 250 to 690 nm with a spectral resolution of 0.8 nm), the third in the 756–773 nm range (with 0.13 nm resolution) and the last in the near infrared (926–952 nm with a spectral resolution of 0.13 nm). The main goal of GOMOS is the global, long-term monitoring of stratospheric and mesospheric ozone. Furthermore, the large wavelength range and the spectral resolutions allow the retrieval of other species like NO_2, NO_3, H_2O, O_2, OClO and aerosol extinction (Bertaux et al., 2010). The following section explains the method used to retrieve OClO.

3 The retrieval of OClO

The starting point of most occultation retrieval algorithms is the well-known Beer–Lambert law. It describes how the signal is affected by the presence of atmospheric absorbers along the line of sight at tangent altitude z:

$$S(\lambda, z) = S_0(\lambda) \exp\left(-\sum_i \sigma_i(\lambda) N_i(z)\right), \quad (1)$$

where σ_i is the extinction cross section and N_i is the slant column density of each atmospheric absorber in the spectral range selected. A detailed overview of the GOMOS operational algorithm can be found in Kyrölä et al. (2010b).

Most of the expected species can be directly retrieved from single measurements but the combination of the weak signal-to-noise ratio of a single GOMOS measurement and the small optical thickness of OClO forces us to combine several single measurements in order to detect it. The retrieval of OClO from GOMOS measurements requires two steps. The first is the calculation of an averaged transmittance spectra and the second is the inversion process of these spectra.

As discussed above, the first step is required to increase the signal-to-noise ratio so that the retrieval of OClO can be carried out in the second step of the process. The idea is to use several co-located (spatially and temporally) GOMOS measurements to build a new measurement. This is possible because each measurement consists of a transmittance and is consequently independent of the selected star. This averaged measurement is supposed to be representative of one particular location for a given moment. For the selection of the GOMOS measurements used to build the averaged measurements, we have used the following steps:

- selection of stars: stars with effective temperatures greater than 4100 K to ensure a sufficient UV flux and stars with magnitudes lower than 2 to have acceptable photon fluxes. These criteria lead to a selection of 44 stars.
- temporal resolution: one month or one year. The time period is September 2002 to the end of 2011. The choice of this temporal bin size is influenced by the latitudinal resolution hereafter. Latitude bands: for the annual climatologies, the latitude range covers latitudes from 80° S to 80° N with 10° latitude bands. For the monthly time series, we have used 20° latitude bands for the regions located between 30° S and 30° N and 30° latitude bands elsewhere to ensure sufficient numbers of measurements in each data set.
- illumination conditions: only dark limb and straylight condition measurements are used. Dark limb condition corresponds to measurements made when the solar zenith angle is higher than 120°. Such measurements can be used without restriction. Measurements are said to be in straylight conditions if the instrument is illuminated by light coming from the scattering of solar light. Straylight measurements are considered as of good quality (more details can be found in the GOMOS product handbook at http://envisat.esa.int/handbooks/gomos/toc.htm).
- the GOMOS data used here are obtained with the version 5 of the ESA level 1 operational processor.
- all the selected spectra are linearly interpolated on a common vertical grid of tangent altitudes from 0 to 60 km with 1 km steps.

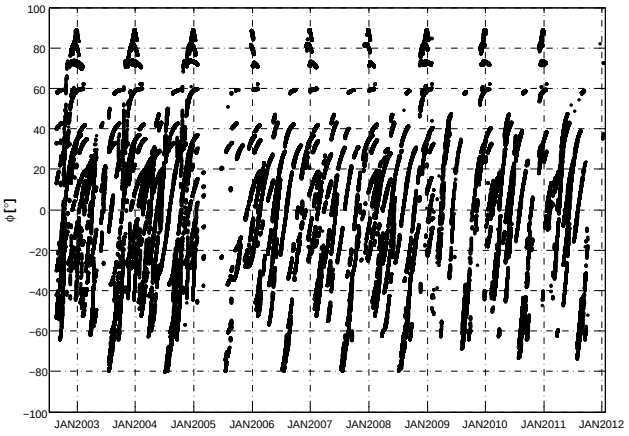

Fig. 2. Latitudinal distribution of the GOMOS transmittance measurements used to retrieve OClO as a function of time.

Figure 2 shows the latitudinal distribution of the GOMOS data used in our study to retrieve OClO. A total number of about 162 000 GOMOS measurements have been processed. While both polar regions are well covered during the winters and much less outside these periods, the other latitudes are very well sampled during all years (except in 2005). During the first months of 2005 (until June), almost no measurements are available due to an instrumental breakdown. However, some measurements in the polar regions could be carried out (particularly in January).

For each bin, we have built a data set: $[T_1(\lambda_i, z_j), \ldots, T_n(\lambda_i, z_j)]$ where z_j are the 61 tangent altitude levels, λ_i are the wavelengths and n is the number of GOMOS measurements in the bin. Once all the data sets are built, they are statistically analyzed to guarantee the homogeneity of the bin data sets and subsequently, to ensure the representativeness of the averaged measurement that will be derived from this data set. For each data set, statistical detections of multimodal distribution are performed by fitting the distribution with theoretical models. Figure 3 shows examples of GOMOS transmittance distributions for a monomodal and a bimodal case. The bimodality observed here in the high latitude band is due to the fact that some measurements are inside the polar vortex and others are outside. In fact, inside the vortex, the air is older than outside. As a result, the air density is smaller inside the vortex and the transmittance inside exceeds the one outside. In addition, a part of this difference can be attributed to the low concentration of NO_2 inside the polar vortex (denoxification). All cases of bimodal distributions observed in our study are due to measurements done inside and outside the polar vortex. In this case, both modes are studied separately and, after visual inspection, we have selected the one that represents the high latitude band, in other words the one inside the polar vortex with greater transmittances (the other modes will be analyzed in the frame of some case studies). Note that another case is possible when the line

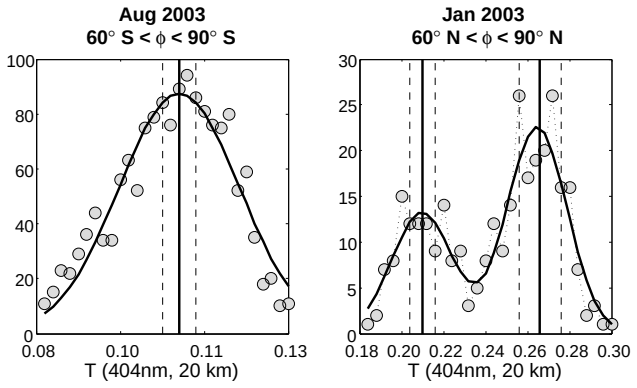

Fig. 3. Example of monomodal (left panel) and bimodal (right panel) distributions of GOMOS transmittance for an altitude of 20 km and a wavelength of 404 nm. The solid curves represent the best fit obtained, the solid vertical lines represent the weighted median for each mode while the dashed lines are the weighted median absolute deviations.

of sight of a single occultation crosses the vortex edge. We do not distinguish this kind of occultation in our study. Thereafter, an outlier detection is performed for each data set using a jackknife method (Quenouille, 1956). Finally, for each tangent altitude and each wavelength, the weighted median transmittance is calculated instead of the mean because the median is known to be more robust against the presence of residual outliers. Furthermore, as the signal-to-noise ratios of different measurements can differ considerably, we combine transmittances weighted with respect to the inverse of their estimated measurement errors. A weighted median calculation starts by sorting the transmittance values in increasing order, and rearranging the associated weights in the same fashion. The cumulative distribution of these weights is subsequently evaluated. The weighted median is then the transmittance value corresponding to the 50 % level of this cumulative weight distribution. The uncertainty associated with the weighted median is calculated as the weighted median absolute deviation (WMAD). It is the median of the absolute value of the difference between each transmittance value and the weighted median. This statistical study ensures that the calculated averaged spectra are representative of the considered region. Figure 1 shows transmittance spectra in the 250–690 nm range for a single oblique occultation, a single vertical occultation and an averaged occultation. We can note that the signs of residual scintillation disappear in the averaged spectra (bottom panel) and that residual scintillations are almost perfectly corrected in the vertical occultation spectra (center panel) whereas some remaining scintillations persist in the oblique spectra (top panel).

The second step consists of a DOAS algorithm applied to averaged transmittance spectra to retrieve all the chemical species involved in the absorption of the radiation in the wavelength range used. The DOAS technique has been reviewed by Platt et al. (1979). The principle of this method is quite simple: it is based on the idea that the transmittance consists of two components, one varying slowly with the wavelength and the other rapidly varying. In the spectral range used, the slowly varying component $T_s(\lambda)$ reflects the Rayleigh scattering, aerosol extinction, polar stratospheric clouds extinction and the slowly varying part of the gaseous absorptions while the second component represents the rapidly varying part of gaseous absorptions. $T_s(\lambda)$ is obtained by fitting the measured transmittance $T(\lambda)$ by a second-order polynomial in the wavelength window selected. Several other functions have been tested and it clearly appears that it is sufficient to use a second-order polynomial to fit the slowly-varying component. After which the experimental differential transmittance $dT(\lambda)$ is simply expressed as the difference between $T(\lambda)$ and $T_s(\lambda)$ while the modeled differential transmittance $M(\lambda)$ is expressed as

$$M(\lambda) = T_s\left(\exp\left[-\sum_j N_{\mathrm{gas}_j}\delta\sigma_{\mathrm{gas}_j}\right]-1\right), \quad (2)$$

where N_{gas_j} and $\delta\sigma_{\mathrm{gas}_j}$ correspond respectively to the SCD and the differential cross sections of the absorber gas in the wavelength interval. $\delta\sigma_{\mathrm{gas}_j}$ is the difference between the absorption cross section of gas j and a second-order polynomial fitting this cross section. Then, at each tangent altitude, an optimization of the modeled differential transmittance is performed to retrieve the SCDs by using a nonlinear least-square minimization of the chi-square merit function $\left(\chi^2\right)$ defined as the difference between $M(\lambda)$ and $dT(\lambda)$ weighted by the measurement errors:

$$\chi^2(z_t) = \sum_{i=1}^{n}\left[\frac{dT(\lambda_i, z_t) - M(\lambda_i, z_t)}{\epsilon(\lambda_i, z_t)}\right]^2, \quad (3)$$

where n is the number of pixels in the fitting window and ϵ is the error associated to the averaged differential transmittance. Once the SCDs are retrieved, the errors made ΔN_{gas} are given by the root square of the diagonal elements of the error matrix **e** (the inverse of the curvature matrix, which is equal to one-half times the Hessian matrix of the chi-square function). More information can be found in Press et al. (2007).

We have studied 4 spectral ranges: 355–381, 355–390, 390–425 and 355–425 nm. For these 4 fitting windows, we have calculated at each tangent altitude z_t the reduced chi square, which is simply the χ^2 used previously divided by the degree of freedom (n minus the number of parameters used in the minimization process). For the fitting windows selected, the reduced chi squares are between about 0.1 and 1.5 (an example is presented in the top left panel in Fig. 4). On the basis of this example, the best chi square ($\chi^2 \approx 1$) is obtained with the interval 355–381 nm for all the altitude range. Moreover, the analysis of the mean of the residual (i.e., the spectral mean of the differences between observed and modeled transmittances) at each tangent altitude shows that below 25 km there is almost no difference; but above, the mean

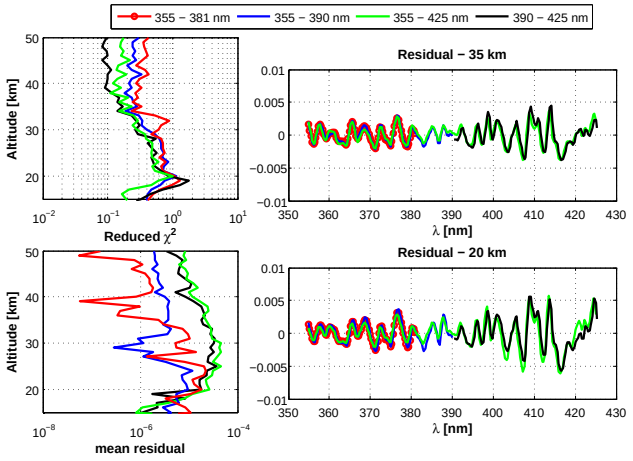

Fig. 4. Left top panel: reduced chi square as a function of altitude. Left bottom panel: mean of the residual as a function of altitude. Right panel: residual transmittance at 35 and 20 km. These figures show results based on the averaged occultation corresponding to the year 2007 in the 70 and 80° S latitude bands.

residual is lower when the 355–381 nm wavelength range is used (bottom left panel in Fig. 4). Furthermore, residuals at each tangent altitude (right panels in Fig. 4) are clearly smaller below 390 nm. The same study has been done using several other averaged occultations and the conclusions are always identical; we have therefore selected the 355–381 nm spectral window. In this spectral range, we have to consider the absorptions of OClO, NO_2 and also O_3 even if its cross section is very small in this range. Thus, these three species are fitted simultaneously. In Fig. 5 (right panel), we show an example of OClO SCDs in the Antarctic region (in blue), in the Arctic region (in black) and in the equatorial region (in red) for the year 2003. The left panel in Fig. 5 shows the vertical profiles of the relative error for these three profiles. The range of the relative errors extends generally from about 5 to 70 %. We can already notice several specific structures that will be discussed in more detail in the following sections. In particular, we can observe the presence of an "OClO SCD peak" in the middle stratosphere in the equatorial regions and the expected chlorine activation in the lower stratosphere in both polar regions with a higher amplitude in the south. The next step is the spatial inversion used to retrieve the vertical profile of concentrations. Nevertheless, we have found that the error bars become too important after the spatial inversion (from 60 to 180 %) and that only the OClO SCDs provide error bars that make the product usable for seasonal or latitudinal studies. As a consequence, the climatologies will be presented both in terms of SCDs and concentrations but the subsequent discussion will be only about columns.

The following section presents a comparison of the OClO GOMOS product with those retrieved using balloon-borne instruments.

4 Comparisons with other instruments

Since the nighttime OClO SCD from GOMOS averaged measurements is a new product, it is necessary to validate it. Nevertheless, since GOMOS is the only satellite instrument able to perform nighttime measurement of OClO, a global validation is difficult to achieve. As a result, the following discussion should be considered as a simple comparison and not as a validation of the GOMOS OClO product. In this comparison exercise, we have excluded O_3 and NO_2 SCDs retrieved using the present algorithm because the spectral window used is not the most appropriate one to perform the retrieval of these species, considered here as interfering species. Nonetheless, as a first analysis of the quality of our products, we can compare NO_2 retrieved from GOMOS averaged measurements and the operational GOMOS data. This has been done previously and published in Tetard et al. (2009). The results (not reproduced here) indicate that there is a very good agreement between both products (typically, relative differences are between −10 and +10 %) and that our method seems to work properly.

The second step consists in comparing the GOMOS OClO products with those from other instruments. The only nighttime OClO profiles available for comparisons are those retrieved from the AMON and SALOMON balloon-borne instruments. One should keep in mind that these comparisons are done between spatially and temporally localized measurements and a composite of several measurements localized in a latitude band. AMON and SALOMON instruments performed nighttime remote sensing measurements using respectively the stellar and the lunar occultation method. They provided slant column densities of OClO. However, since the observation geometries of GOMOS and of balloon-borne instruments are different, it is not appropriate to compare directly the slant column densities but instead to compare the OClO concentration vertical profiles even if the associated uncertainties are important. To do so, we had to perform spatial inversion of the SCDs. For GOMOS, this has been done by using an onion peeling method. The atmosphere is divided into concentric layers that are assumed to be homogeneous. Using the matrix formalism, the problem consists of solving the following linear system:

$$\mathbf{N} = \mathbf{K}\mathbf{n}, \tag{4}$$

where the matrix elements of **N** are the OClO SCDs at each tangent altitude, **K** is the path length matrix (a triangular matrix) and **n** is the OClO vertical profile matrix. The GOMOS spatial inversion is a well-conditioned problem and is easy to solve by using standard methods. Nevertheless, it is important to repeat that this exercise of comparison is not a validation but just a simple verification. In fact, the uncertainties associated to OClO concentrations are generally too large to be used scientifically.

AMON is a UV–visible spectrometer that uses the stellar occultation method. The flights used took place on 1

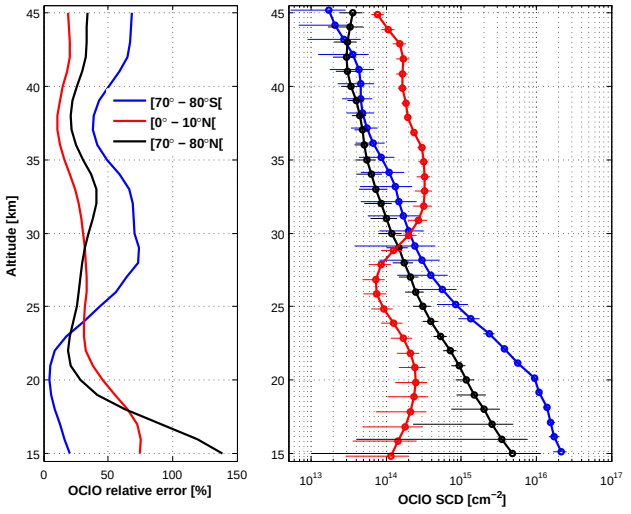

Fig. 5. Right panel: OClO SCD profiles retrieved from GOMOS averaged transmittance for the year 2003 in the Antarctic region (in blue), the Arctic region (in black) and in the equatorial region (in red). Error bars represent the retrieval random errors. Profiles have been slightly shifted vertically for clarity. Left Panel: vertical profiles of OClO relative error.

and 3 March 2003 in Kiruna, northern Sweden (latitude 67°53′ N, longitude 21°05′ E). We have used the measurements from the occultation of Sirius (α Canis Majoris) and Alnilam (ϵ Orionis). Both stars emit enough UV radiation to detect OClO (effective temperatures are respectively 11 000 and 30 000 K).

The second balloon-borne instrument used is SALOMON (Renard et al., 2000). It is a UV–visible spectrometer that uses the lunar occultation method. The flight occurred in January 2006 in Kiruna and the measurements were done during the balloon ascent inside the polar vortex. The OClO concentration profile from the SALOMON measurements has been studied by comparisons with the results of the model described in Berthet et al. (2007). In particular, they have shown that the OClO product from SALOMON is in acceptable agreement with results from chemistry transport model calculations.

For the inter-comparisons, the GOMOS measurements used to build the averaged measurements were located between 60 and 75° in a 20 day window centered on the flight date. Only the GOMOS measurements of year of the correlative balloon flights have been used. The statistical analysis has revealed no bimodal distribution. Since the GOMOS' vertical resolution is close to the AMON and SALOMON resolutions, no smoothing procedure was required and direct comparisons could be done.

Figure 6 shows the results of these comparisons. The curves on the left concern the comparisons with AMON and show a satisfactory agreement. The maxima are reached at approximatively the same altitudes for the three profiles (19 km). The value of the maximum of OClO concentration is almost identical for the GOMOS and the AMON (ϵ-ORI) profiles but is higher for the AMON (α-CMA) profile: 5.3×10^7 cm^{-3}, 4.2×10^7 cm^{-3} and 1×10^8 cm^{-3} respectively. The corresponding errors are respectively 5.7×10^7 cm^{-3}, 7.2×10^6 cm^{-3} and 5.7×10^6 cm^{-3} The differences in concentration could be explained by asserting that the OClO concentrations can vary according to the area of the vortex observed. A secondary maximum is observed in the three profiles at almost the same altitudes: 26 km for GOMOS and AMON (ϵ-ORI) and 26.5 km for AMON (α-CMA). Here again, the concentration values reached are almost identical for the GOMOS and the AMON (ϵ-ORI) profiles (respectively 1.6×10^7 and 1.8×10^7 cm^{-3}) whereas the AMON (α-CMA) profile exhibits a higher value: 2.5×10^7 cm^{-3}. Error bars are respectively 2×10^7 cm^{-3}, 4×10^5 cm^{-3} and 5.4×10^6 cm^{-3}. Overall, the OClO profile from the GOMOS averaged measurement is closer to the product of AMON when ϵ-ORI is occulted: for most of the altitude range, the AMON (ϵ-ORI) profiles are well within the GOMOS error bars.

Concerning the comparisons with SALOMON (right panel in Fig. 6), the agreement is less encouraging. The first maximum is reached at about 20 km for SALOMON and at 18 km for GOMOS. This difference can be attributed to the fact that the peak height can vary according to the location of the measurement in the polar vortex. The maximum of OClO concentration measured by SALOMON is twice the one retrieved by GOMOS (1.2×10^8 and 6.1×10^7 cm^{-3} respectively and errors are 2.6×10^6 cm^{-3} and 1×10^8 cm^{-3}). Moreover, above 28 km, the SALOMON concentrations increase strongly, reaching a value of 1.3×10^8 cm^{-3} ($\pm 4.5 \times 10^7$) at 32 km whereas the OClO concentrations from GOMOS are always decreasing.

In summary, the OClO product from GOMOS averaged measurements compares very well with that from AMON measurements and slightly less well with that of SALOMON. Overall, the conclusion is that our OClO product is of sufficient quality for some scientific uses such as seasonal or latitudinal studies and needs a more thorough validation for some others (comparisons with models for example).

5 Climatology of OClO

5.1 Annual climatology

As specified previously, we use 10° latitude bins for the annual climatologies. For each altitude, the distribution of OClO SCDs with latitude are fitted by one or two Lorentzian function(s), taking into account the retrieval errors. The choice of Lorentzian functions to fit the latitudinal variations of the OClO SCDs is based on the fact that for a few dozen examples, the best fit was achieved using this kind of function (Gaussian and Pearson functions had been also tested).

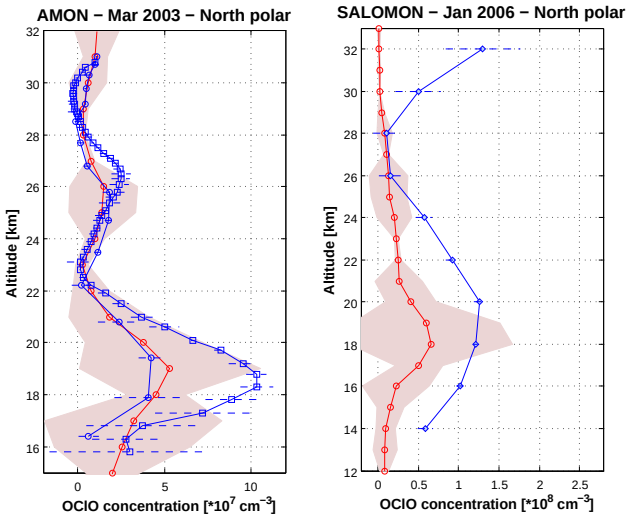

Fig. 6. Left: vertical profiles of OClO concentrations retrieved from GOMOS averaged measurements (in red) and from AMON measurements on 1 and 3 March 2003 (blue square for α CMA occultation and circle for ϵ ORI occultation). Right: comparisons with a SALOMON measurement (in blue) on 16 January 2006. The shaded area and the horizontal bars represent the associated errors.

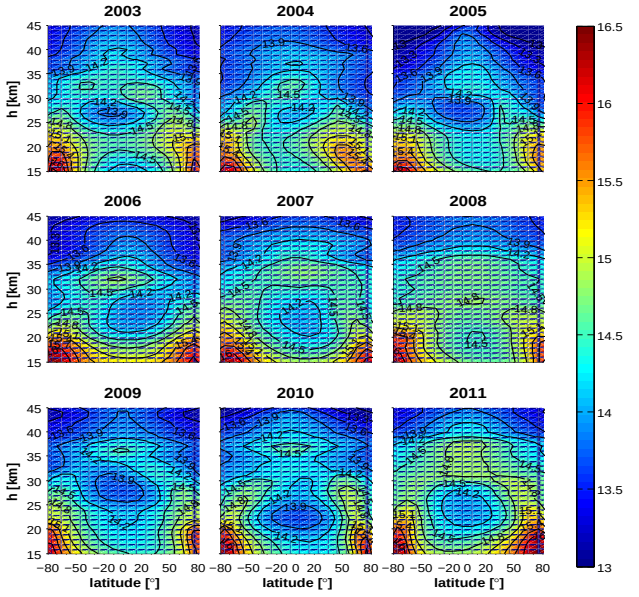

Fig. 7. Latitude–altitude maps of OClO slant column densities (log scale, cm^{-2}) retrieved from GOMOS measurements for years 2003–2011. Latitude range of 80° S–80° N, altitude range of 15–45 km.

In Fig. 7, we present the isopleths of the latitude–altitude OClO slant column densities (log scales) for years 2003–2011 and the same maps but in concentration are presented in Fig. 8. The altitude range is limited from 15 to 45 km. Outside this range, either the retrieval does not succeed or the uncertainties of the retrieval are too large. The 9 latitude–altitude maps of OClO SCDs presented in Fig. 7 show approximately the same structure. The following discussion concerns the slant column densities because the errors associated with the concentration climatologies are too large (mean value of about 90 % and upper limit of 180 %). In the lower stratosphere, we can observe high values in the polar regions, reaching about 10^{16} cm^{-2} in the Southern Hemisphere and generally slightly less in the north (about 10^{15} cm^{-2}). These high values are expected (Eq. R1) and are an indication of the chlorine activation that occurs in spring (in the Northern Hemisphere) and in fall (in the Southern Hemisphere). At higher altitude in the polar regions OClO SCDs decrease abruptly for all years. This decrease can be explained by the scarcity of ClO at these altitudes. This is well observed by the Microwave Limb Sounder (MLS) instrument onboard the satellite platform AURA (see plots available at http://mls.jpl.nasa.gov). Note that the concentration maps (Fig. 8) exhibit the same structures.

In the equatorial region, an OClO SCD peak is present all year between about 30 and 35 km. The latitudinal extent as well as the maxima of the layer is somewhat variable from one year to another. The fact remains that the maxima are about a few 10^{14} cm^{-2}. The location of the maxima is approximately around the Equator. Note that the year 2011 exhibits the stronger OClO equatorial SCD peak (the maxima is nearly 10^{15} cm^{-2}). The OClO equatorial stratospheric SCD peak was first discovered by Fussen et al. (2006) for the year 2003. A possible explanation for the presence of OClO at these altitudes can be the low pressure at these levels, which make the 3-body reactions between ClO/BrO and NO_2 (R4 and R5) less effective. Thus, the reaction (R1) between ClO and BrO becomes dominant and explains the presence of OClO. Moreover, the satellite instrument MLS confirms the presence of a ClO layer in the upper stratosphere in the equatorial region. One may notice the more extended (in terms of altitude) OClO SCD peak for the years 2008 and 2011. Finally, the OClO SCDs decrease progressively above this layer. The other latitude regions are characterized by weak OClO values. Consequently, in the following, our attention will be focused on equatorial and polar regions.

5.2 Monthly climatology of OClO

In Fig. 9 we show the time series of OClO SCDs in three latitude bands: the equatorial band (10° S–10° N, middle panel), the north polar band (60–90° N, top panel) and the south polar band (60–90° S , bottom panel). In the equatorial region, the missing data in 2005 are due to a GOMOS failure. The discontinuity observed in the two polar time series are due to the spatial coverage of GOMOS at these altitudes (cf. Fig. 2). Figure 10 exhibits the same time series but the color scale corresponds to OClO concentrations.

Regarding the northern latitude band, we can clearly observe an annual increase of OClO followed by a decrease

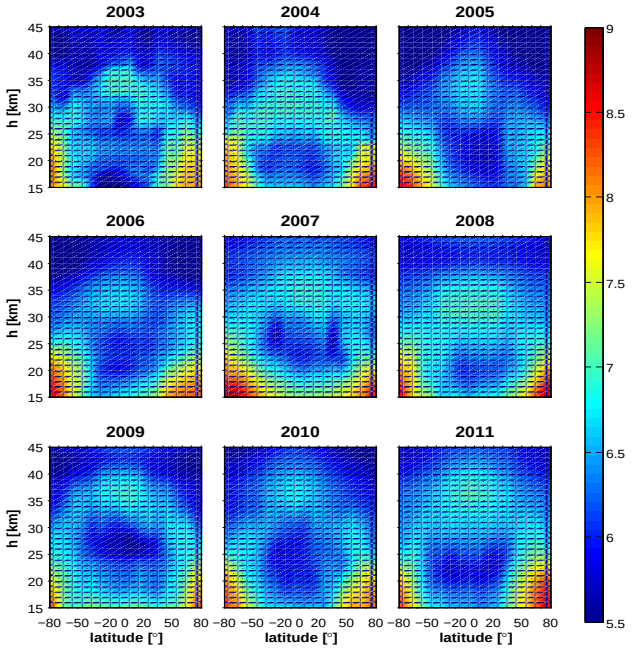

Fig. 8. Same as Fig. 7 but latitude–altitude maps of OClO concentration (log scale, cm^{-3}) are presented. Note that errors associated are very large (from 60 to 180 %)

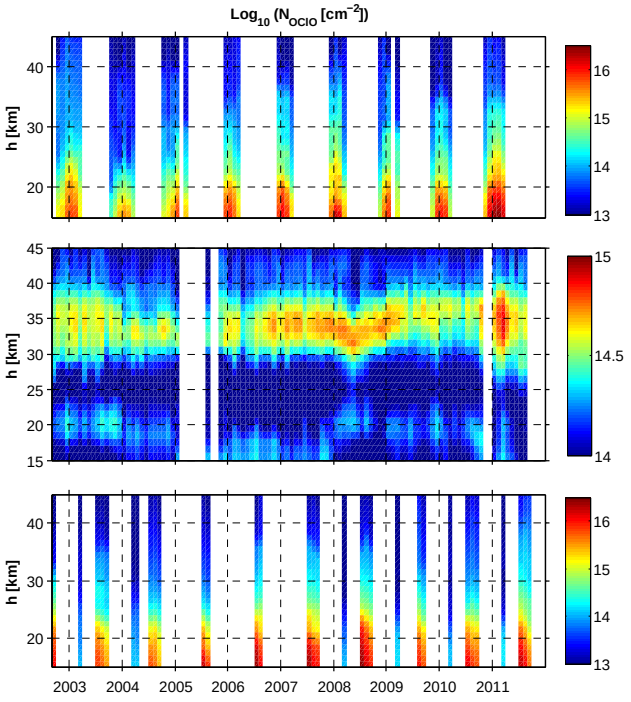

Fig. 9. Monthly OClO slant column densities (log scale, cm^{-2}) in three latitude bands for the period from September 2002 to December 2011. Latitude bands: 60–90° N (top), 10° S–10° N (middle) and 60–90° S (bottom). The color scales used are the same for the two polar time series but differ for the equatorial time series.

in the lower stratosphere (below about 25 km). The increase begins in December and reaches a maximum of about 5×10^{15} cm^{-2} to 3×10^{16} cm^{-2}. The corresponding OClO concentrations (obtained after the spatial inversion described in Sect. 4) are 5×10^7 to 2×10^8 cm^{-3}. This is in good agreement with the values previously observed with other instruments (summarized in Table 1). Regarding the altitude of the maximum of OClO SCDs, the values obtained using GOMOS measurements (about 17 km) are generally lower than those found by the balloon-borne instruments. The high OClO values are the sign of chlorine activation in the winter polar vortex. Note that the year 2011 shows strong OClO values in the lower stratosphere. Indeed, the ozone depletion in the Arctic winter 2010/2011 has been one of the most severe of the last decade (Kuttippurath et al., 2012). This feature is also observed in the corresponding annual isopleth (Fig. 7).

For the south polar region (bottom panel in Fig. 9), only a few months of each year can be analyzed (from July to September and for some years, in February and March). Typically, the time series shows high OClO values from July to September indicating the sign of chlorine activation. The OClO SCD maximum reached in the Antarctic regions (from 1.5×10^{16} to 5.7×10^{16} cm^{-2}) are larger than those observed in the Arctic regions. This is well illustrated in Fig. 11 showing these OClO SCD maxima for winters of 2003–2011. The maximum concentrations range from 7×10^7 cm^{-3} to 3×10^8 cm^{-3}. Unfortunately, we cannot validate our values because of the lack of occultation measurements in the south polar region.

The equatorial region (middle panel in Fig. 9) is characterized by an OClO SCD peak between about 30 and 40 km for each year. There are too few values available in 2005 to discuss this year. In the middle stratosphere, the OClO SCD maximum is located at about 35 km for the years 2003, 2006, 2007 and 2009–2011. For the years 2004 and 2008, the maximum is located slightly lower, around 32 km. This SCD peak appears to be present during the entire year with only small variations.This is in good agreement with the results obtained by the MLS instrument, which shows a quasi-constant ClO layer at these altitudes with a volume mixing ratio of 0.3–0.4 ppbv, corresponding to concentrations of 2×10^7 to 3×10^7 cm^{-3}. Note that a stronger OClO SCD peak is observed for periods ranging from late 2006 to early 2009 (on average 5×10^{14} cm^{-2}, uncertainty about 21%) and at the beginning of 2011 (on average 5.5×10^{14} cm^{-2}, uncertainty about 25 %). By excluding these two periods, an average background level has been calculated and the maximum computed is equal to 3.6×10^{14} cm^{-2} (uncertainty about 9 %). Taking into account the associated uncertainties, these two enhancements are statistically significant. Further studies are needed to analyze and interpret these observations in cooperation with modelers. As expected, almost no OClO is detected in the lower part of the stratosphere.

Table 1. Maximum of OClO concentrations previously detected by balloon-borne instruments and by GOMOS during nighttime in the Arctic polar vortex. The altitude of the maximum is also indicated.

Instrument	Date	$[OClO]_{max}$ (cm^{-3})	Alt (km)	Comments
AMON	Feb 1995	8.7×10^7	19	Renard et al. (1997)
	Mar 2003	5.3×10^7	19	
		1.0×10^8	19	
SALOMON	Jan 2000	8.7×10^7	18	Riviere et al. (2003)
	Jan 2006	1.2×10^8	20	Berthet et al. (2007)
GOMOS	2003–2011	5×10^7 to 2×10^8	17	this work

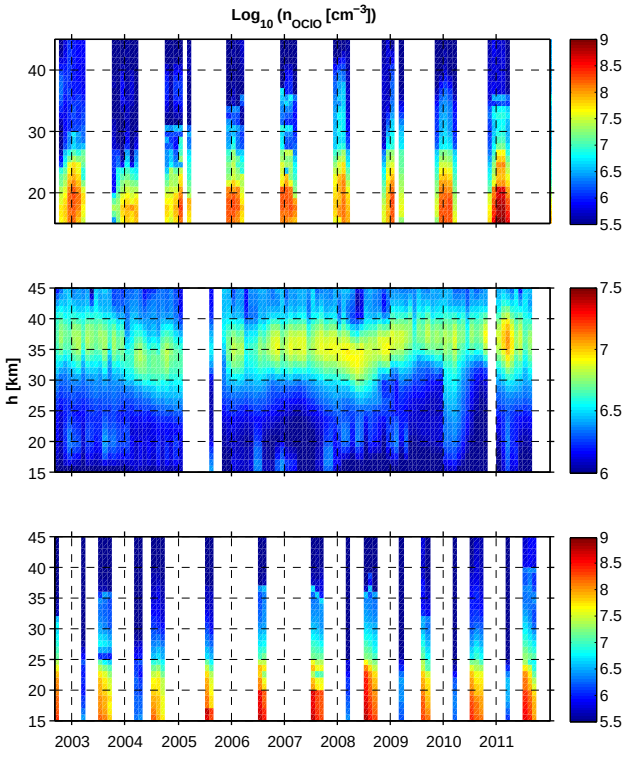

Fig. 10. Same as Fig. 9 but monthly OClO concentrations (log scale, cm^{-3}) are presented.

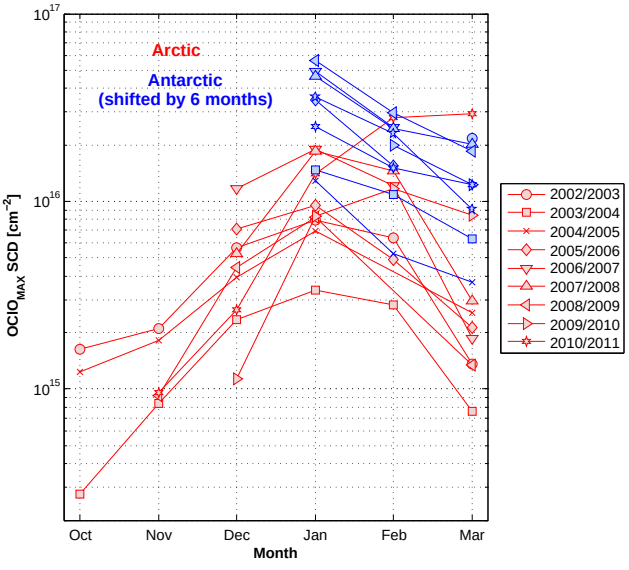

Fig. 11. Maximum monthly OClO SCDs in the Arctic regions (in red) and in the Antarctic regions (in blue) for the winters of 2003–2011. For comparisons with the Arctic OClO SCDs, the Antarctic OClO values have been shifted by 6 months.

6 Conclusions

In this article, we have presented an innovative method to retrieve small absorber constituent. This method is applied to the GOMOS measurements to detect OClO. It consists of the combination of several co-located GOMOS measurements to build one measurement with a higher signal-to-noise ratio. Then a specified algorithm is used to retrieve OClO slant column densities.

We have compared our results with those obtained using balloon-borne instruments AMON and SALOMON. It appears that our OClO product is in a very good agreement with the AMON product and compares slightly less well with SALOMON. Therefore, the quality of this product is sufficient for seasonal or latitudinal studies.

We have constructed climatologies of OClO based on annual binning. It clearly appears that the same structures emerge every year. First, in the polar regions, we systematically observed a strong annual cycle of OClO in the lower stratosphere. This is related to the activation of the chlorine species in the polar vortex. Moreover, an OClO SCD peak in the equatorial region is clearly detected each year in the middle stratosphere. This peak is the result of the reaction between BrO and ClO effectively detected at these altitudes by the MLS instrument.

Time series of OClO SCDs have been built using averaged measurements representative of one month for three latitude bands corresponding to Arctic, Antarctic and equatorial regions. The period of these climatologies is from 2003 to 2012, covering the entire GOMOS mission. It appears that activation of chlorine species is well observed in the winter

pole. Furthermore, the OClO SCD peak in the equatorial middle stratosphere is detected during all the years studied and presents no major variations.

The next step of these studies will be a complete validation of the GOMOS OClO product by using satellite instruments (OSIRIS, SCHIAMACHY) and photo-chemical models. Then, we will use models to interpret quantitatively the results presented in this article. The method presented here is promising and could be applied to other instrumental data. In addition, it can be used to detect other weak absorbers such as BrO. The climatology presented in this paper can be considered as the first and only long-term nighttime OClO climatology that exists at present.

Acknowledgements. This study was funded by the PRODEX/ RADIAL (PEA 4000102793) contract under the authority of the Belgian Space Science Office (BELSPO).
We thank the AMON and SALOMON science team for giving us the authorization to use their OClO concentration profiles.

Edited by: R. Schofield

References

Bertaux, J. L., Kyrölä, E., Fussen, D., Hauchecorne, A., Dalaudier, F., Sofieva, V., Tamminen, J., Vanhellemont, F., Fanton d'Andon, O., Barrot, G., Mangin, A., Blanot, L., Lebrun, J. C., Pérot, K., Fehr, T., Saavedra, L., Leppelmeier, G. W., and Fraisse, R.: Global ozone monitoring by occultation of stars: an overview of GOMOS measurements on ENVISAT, Atmos. Chem. Phys., 10, 12091–12148, doi:10.5194/acp-10-12091-2010, 2010.

Berthet, G., Renard, J. B., Catoire, V., Chartier, M., Robert, C., Huret, N., Coquelet, F., Bourgeois, Q., Riviere, E. D., Barret, B., Lefevre, F., and Hauchecorne, A.: Remote sensing measurements in the polar vortex: comparison to in situ observations and implications for the simultaneous retrievals and analysis of the NO_2 and OClO species, J. Geophys. Res., 112, D21310, doi:10.1029/2007JD008699, 2007.

Damiani, A., Funke, B., Marsh, D. R., López-Puertas, M., Santee, M. L., Froidevaux, L., Wang, S., Jackman, C. H., von Clarmann, T., Gardini, A., Cordero, R. R., and Storini, M.: Impact of January 2005 solar proton events on chlorine species, Atmos. Chem. Phys., 12, 4159–4179, doi:10.5194/acp-12-4159-2012, 2012.

Farman, J. C., Gardiner, G., and Shanklin, J. D.: Large losses of total ozone in antartica reveal seasonal ClO_x/NO_x interaction, Nature, 315, 207–210, 1985.

Fussen, D., Vanhellemont, F., Dodion, J., Bingen, C., Mateshvili, N., Daerden, F., Fonteyn, D., Errera, Q., Chabrillat, S., Kyrölä, E., Tamminen, J., Sofieva, V., Hauchecorne, A., Dalaudier, F., Bertaux, J.-L., Renard, J.-B., Fraisse, R., d'Andon, O. F., Barrot, G., Guirlet, M., Mangin, A., Fehr, T., Snoeij, P., and Saavedra, L.: A global OClO stratospheric layer discovered in GOMOS stellar occultation measurements, Geophys. Res. Lett., 33, L13815, doi:10.1029/2006GL026406, 2006.

Krecl, P., Haley, C. S., Stegman, J., Brohede, S. M., and Berthet, G.: Retrieving the vertical distribution of stratospheric OClO from Odin/OSIRIS limb-scattered sunlight measurements, Atmos. Chem. Phys., 6, 1879–1894, doi:10.5194/acp-6-1879-2006, 2006.

Kühl, S., Pukite, J., Deutschmann, T., Platt, U., and Wagner, T.: SCIAMACHY limb measurements of NO_2, BrO and OClO. Retrieval of vertical profiles: Algorithm, first results, sensitivity and comparison studies, Adv. Space Res., 42, 1747–1764, 2008.

Kuttippurath, J., Godin-Beekmann, S., Lefèvre, F., Nikulin, G., Santee, M. L., and Froidevaux, L.: Record-breaking ozone loss in the Arctic winter 2010/2011: comparison with 1996/1997, Atmos. Chem. Phys., 12, 7073–7085, doi:10.5194/acp-12-7073-2012, 2012.

Kyrölä, E., Tamminen, J., Sofieva, V., Bertaux, J. L., Hauchecorne, A., Dalaudier, F., Fussen, D., Vanhellemont, F., Fanton d'Andon, O., Barrot, G., Guirlet, M., Mangin, A., Blanot, L., Fehr, T., Saavedra de Miguel, L., and Fraisse, R.: Retrieval of atmospheric parameters from GOMOS data, Atmos. Chem. Phys., 10, 11881–11903, doi:10.5194/acp-10-11881-2010, 2010b.

Miller, H. L. J., Sanders, R. W., and Solomon, S.: Observations and interpretation of column OClO seasonal cycles at two polar sites, J. Geophys. Res., 104, 18769–18783, 1999.

Oetjen, H., Wittrock, F., Richter, A., Chipperfield, M. P., Medeke, T., Sheode, N., Sinnhuber, B.-M., Sinnhuber, M., and Burrows, J. P.: Evaluation of stratospheric chlorine chemistry for the Arctic spring 2005 using modelled and measured OClO column densities, Atmos. Chem. Phys., 11, 689–703, doi:10.5194/acp-11-689-2011, 2011.

Platt, U., Perner, D., and Pätz, H. W.: Simultaneous measurement of atmospheric CH_2O, O_3, and NO_2 by differential optical absorption, J. Geophys. Res., 84, 6329–6335, doi:10.1029/JC084iC10p06329, 1979.

Press, W. H., Teukolsky, S. A., Vetterling, W. T., and Flannery, B. P.: Numerical Recipes, the art of computing, third edition, Cambridge University Press, 2007, ISBN-10: 0521880688, 2007.

Quenouille, M. H.: Notes on bias in estimation, Biometrika, 43, 353–360, 1956.

Renard, J. B., Lefevre, F., Pirre, M., Robert, C., and Huguenin, D.: Vertical profile of night-time stratospheric OClO, J. Atmos. Chem., 26, 65–76, 1997.

Renard, J. B., Chartier, M., Robert, C., Chalumeau, G., Berthet, G., Pirre, M., and Pommereau, J. P.: SALOMON: a new, light, balloon–borne UV visible spectrometer for nighttime observations of stratospheric trace gas species, Appl. Optics, 39, 386–392, 2000.

Riviere, E. D., Pirre, M., Berthet, G., Renard, J. B., Taupin, F. G., Huret, N., and Chartier, M.: On the interaction between nitrogen and halogen species in the Arctic polar vortex during THESEO and THESEO 2000, J. Geophys. Res., 108, 8311, doi:10.1029/2002JD002087, 2003.

Riviere, E. D., Pirre, M., Berthet, G., Renard, J. B., and Lefevre, F.: Investigating the halogen chemistry from the high-latitude nighttime stratospheric measurements of OClO and NO_2, J. Atmos. Chem., 48, 261–282, 2004.

Salawitch, R. J., Wofsy, S. C., Gottlieb, E. W., Lait, L. R., Newman, P. A., Schoeberl, M. R., Loewenstein, M., Podolske, J. R., Strahan, S. E., Proffitt, M. H., Webster, C. R., May, R. D., Fahey, D. W., Baumgardner, D., Dye, J. E., Wilson, J. C., Kelly, K. K., Elkins, J. W., Chan, K. R., and Anderson, J. G.: Chemical loss of ozone in the Arctic polar vortex in the winter of 1991–1992, Science, 261, 1146–1149, doi:10.1126/science.261.5125.1146, 1993.

Sofieva, V. F., Kan, V., Dalaudier, F., Kyrölä, E., Tamminen, J., Bertaux, J.-L., Hauchecorne, A., Fussen, D., and Vanhellemont, F.: Influence of scintillation on quality of ozone monitoring by GOMOS, Atmos. Chem. Phys., 9, 9197–9207, doi:10.5194/acp-9-9197-2009, 2009.

Solomon, S., Garcia, R. R., Rowland, F. S., and Wuebbles, D. J.: On the depletion of antarctic ozone, Nature, 321, 755–758, 1986.

Solomon, S., Mount, G. H., and Sanders, R.W. Schmeltekopf, A. L.: Visible spectroscopy at McMurdo station, Antartica 2. Observations of OClO, J. Geophys. Res., 92, 8329–8338, 1987.

Solomon, S.: Stratospheric ozone depletion: A review of concepts and history, Rev. Geophys., 37, 275–316, doi:10.1029/1999RG900008, 1999.

Tétard, C., Fussen, D., Bingen, C., Capouillez, N., Dekemper, E., Loodts, N., Mateshvili, N., Vanhellemont, F., Kyrölä, E., Tamminen, J., Sofieva, V., Hauchecorne, A., Dalaudier, F., Bertaux, J.-L., Fanton d'Andon, O., Barrot, G., Guirlet, M., Fehr, T., and Saavedra, L.: Simultaneous measurements of OClO, NO_2 and O_3 in the Arctic polar vortex by the GOMOS instrument, Atmos. Chem. Phys., 9, 7857–7866, doi:10.5194/acp-9-7857-2009, 2009.

Wagner, T., Wittrock, F., Richter, A., Wenig, M., and Burrows, J. P., and Platt, U.: Continuous monitoring of the high and persistent chlorine activation during the Arctic winter 1999/2000 by the GOME instrument on ERS-2, J. Geophys. Res., 107, 8267, doi:10.1029/2001JD000466, 2002.